X-ray emission from layered media irradiated by an x-ray free-electron laser

O. Peyrusse*
Aix-Marseille Université, CNRS UMR 7345, PIIM Marseille, France

P. Jonnard, K. Le Guen, and J.-M. André
Sorbonne Université, Faculté des Sciences et Ingénierie, UMR CNRS, Laboratoire de Chimie Physique–Matière et Rayonnemment, 4 Place Jussieu, F-75252 Paris cedex 05, France

(Received 9 July 2019; revised manuscript received 7 October 2019; published 17 January 2020)

This article presents a computational study of the x-ray fluorescence induced by the irradiation of thin layered media by intense, short x-ray pulses. The treatment is based on a numerical solution of the Helmholtz wave equation both for the pump and for the fluorescence signal. Consistently with a possible heating of the medium during the x-ray pulse, complex refractive indices are calculated at each time step from the results of an underlying treatment of atomic physics. In the context of an important core-hole production as a result of photoionization, we discuss the peculiarities of the resulting amplified fluorescence grazing emission and of the Bragg diffraction which can be realized at some angles inside a multilayer material or even in a perfect crystal.

DOI: 10.1103/PhysRevA.101.013818

I. INTRODUCTION

Quantum optics is itself a broad research field with many applications. More recently, with the developments in synchrotron-radiation optics and the advent of x-ray free-electron lasers (XFELs), x-ray quantum optics has also become a rich research field [1,2]. If soft x rays and x rays interact mainly with inner-shell atomic electrons in atoms, molecules, or solids, hard x rays and γ rays interact with nuclei. Accordingly, one can also mention the advent of nuclear quantum optics [3,4].

Here our concern is the study and the control of radiative emission of matter from cavities or photonic crystals, which is an important tool in modern quantum optics. The x-ray range is particularly important because of its application to the probing of solids and molecules in order to get information on spatial and electronic structures. However, compared with the optical range, the control of x-ray emission is difficult and complex. In this context, one notices that unlike bulk materials, x-ray radiation from a layered or a thin layer material is subjected to interferences inside the medium. As a consequence, the outgoing intensity shows characteristic angle-dependent modulations or oscillations which offer the possibility of control [5,6]. For instance, in a one-dimensional (1D) periodic structure with enough number of layers with different refractive indices, multiple reflection and refraction of x rays cause multiple interferences offering the possibility of tailoring both the exciting radiation and the x rays emitted by fluorescence. Moreover, severeral important phenomena are the consequence of the interaction of x rays with flat surfaces or thin materials at glancing angles. Then, resonance-enhanced x rays can be obtained between parallel surfaces [5]. Again, this effect is the consequence of the constructive interferences when, under certain conditions, x rays are bounced back and forth between two interfaces. In both cases, this kind of cavity effect is no different from standing waves appearing in grazing exit x-ray fluorescence (GEXRF) [7,8] and Bragg scattering of x-ray fluorescence (Kossel diffraction [9], and references therein [10]). Then, by adjusting thicknesses and materials, whether in single thin films or multilayered materials, large electric field (E-field) enhancements can be obtained.

In this context of thin films or multilayered film devices, many applications exist [11]. Among them one notes the characterization of thin films thanks to the sensitivity of the E-field to film thickness, the characterization of solid-solid or solid-liquid interfaces [12,13] by enhancing the signal from the narrow interfacial regions, or the study of the topology of membrane proteins whose weak response may become measurable [5]. Another application is the x-ray core-hole spectroscopy in complex materials. For instance, using the fact that transition metal atoms are active sites in many materials, the spectroscopy of $K\alpha$, β emissions is used to get information on the neighboring atoms through the shift of these lines. One notes that more detailed structural information can be obtained from valence-to-core transitions since they reflect the occupied density of state. Because these transitions are much weaker than pure inner-shell transitions, an enhancement of signal is desirable.

At this step, we did not discuss the nature of the *exciting* devices which can be a source of electrons, of protons, or a source of x-ray photons (tubes, synchrotrons, XFELs). Among these photon sources, the latter enable one to study new states of matter in unprecedented conditions of excitation thanks to their accordability and to the high number of photons available in short bursts. Precedent studies using XFEL sources have shown the possibility of obtaining stimulated emission effects in gases [14], solids [15–17], and liquids [18]. In this article, we present consistent calculations combining

*olivier.peyrusse@univ-amu.fr

the x-ray interference effects in thin films or multilayered materials which are mentioned above, with a strong excitation as provided by an XFEL. In particular, we discuss the possibility of having a strong E-field enhancement of x-ray fluorescence in a context where strong population inversions may occur. The effect of the pump is taken into account not only in the excitation process but also in the inherent heating of the material. First, Sec. II discusses the theoretical aspects of the underlying physics involved. We present successively, the problem of the interaction of x rays with a material, how one calculates the exciting x-ray field in the material, and the resulting x-ray field associated with fluorescence. Section III presents in more detail, the specific and distinct types of x-ray effects (GEXRF and Kossel diffraction) as mentioned in this Introduction. In Sec. IV, we turn to the context of XFEL irradiation (and excitation) where the combination of x-ray interference effects and population inversion leads to specific effects on x-ray fluorescence. Several illustrations of these features are presented. Section V summarizes these results and gives a discussion for further studies.

II. BASIC THEORETICAL ASPECTS

Because of the small thickness of the samples considered here, and specifically looking for standing-wave effects, our goal is to get an E-field map inside a particular material. Both for the excitation field and the fluorescent x-ray fields, one has to solve a wave equation for the E-field. Considering one-photon processes, the response of the medium relies on a basic local quantity, which is the complex refractive index $\tilde{n}$. $\tilde{n}$ is usually defined as $\tilde{n} = 1 - \delta - i\beta$, where δ is related to the dispersion and β to the absorption of radiation. It is well known that x rays are totally reflected by a flat surface at small angle of incidence $\theta_{\text{inc}} < \theta_c$ where the critical angle θ_c is defined so that $\theta_c = \sqrt{2\delta}$. As we will see below, resonant wave effects may occur in the vicinity of θ_c for an outgoing wave (at θ_{out}) originating from the material. In a multilayered periodic material, strong interference effects are also expected in the vicinity of the Bragg angle defined by $\Lambda \sin\theta_B = \lambda/2$ (Λ being the *period* of the material). Then, for both $\theta_{\text{out}} \sim \theta_c$ and $\theta_{\text{out}} \sim \theta_B$, a precise determination of the E-field is required.

A picture describing a multilayer sample or simply an inhomogeneous 1D material discretized in different cells, is given in Fig. 1. For a given wavelength, each layer has its own refractive index. Here, we consider separately the problem of a monochromatic plane wave incident on the sample, and the problem of a monochromatic plane wave emitted by the sample. The former corresponds to the excitation XFEL field (pump at ω_p) while the latter corresponds to the fluorescence field (at ω_f). Depending on the polarization and on the angle of incidence, a part of the pump wave is reflected while the other propagates or is absorbed in the medium. The electric field separates into two components: component S (along the z axis) and component P (in plane xy). Moreover, depending on the glancing angle and for both polarizations (S, P), a wave corresponding to the fluorescence field is emitted in the forward and the backward directions (with respect to the pump). Whether for the pump field or for the fluorescence field, the slowly varying envelope approximation allows one

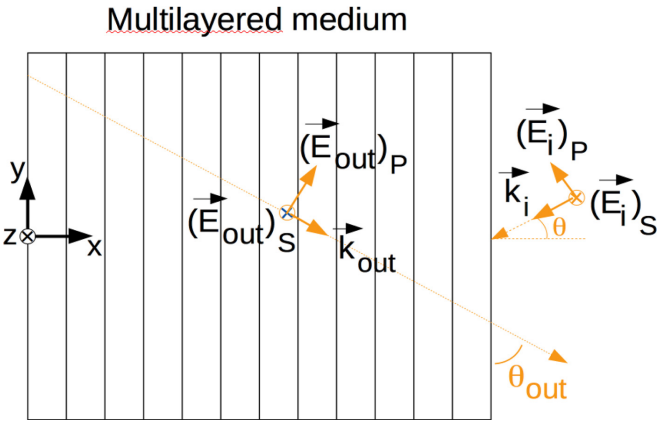

FIG. 1. Schematic diagram of a multilayered material irradiated by a plane wave in the x-ray range. $\vec{E}_i$ is the incident electric field (excitation field or *pump*). $\vec{k}_i$ is the corresponding wave vector. A reflected and a transmitted field also exist (not indicated in the figure). $\vec{E}_{\text{out}}$ is the outgoing (fluorescent) electric field. By virtue of the reciprocity theorem, it is calculated in a similar way to the incident field but at the fluorescence wavelength. θ_{out} is the glancing angle of detection. An electric field separates into two components: S (along the z axis) and P (in the plane xy).

to write each component of the electric field as $E_i = \tilde{E}_i \exp i\omega t$ where i stands for (x, y, z) and where $\omega = \omega_p$ or ω_f. Starting from the wave equation $\Delta E_i + \frac{\tilde{n}^2}{c^2}\frac{\partial^2 E_i}{\partial t^2} = 0$, noting that $\frac{\partial \tilde{E}_i}{\partial t}$ is negligible compared with $\omega\tilde{E}_i$ for keV photons and neglecting propagation effects (given the small thicknesses considered here), components of the envelope obey the Helmholtz wave equation

$$\Delta\tilde{E}_i + \frac{\omega^2}{c^2}\tilde{n}^2(\omega)\tilde{E}_i = 0. \tag{1}$$

The time variation Δt of the refractive index (which follows the XFEL pulse) is typically of the order of 1 fs. Therefore, neglecting propagation effects precludes the study of samples of thicknesses greater than $c\Delta t$. Equation (1) must be solved at each instant for a given x-ray pulse. As a consequence, $\tilde{n}(\omega)$ must be calculated beforehand at each instant in each layer (or cell) of the sample. As shown in Fig. 1, discretization of the medium is along x while the propagation is in the plane (xy). Consequently, in polarization S, one follows only component $\tilde{E}_z$ written as $\tilde{E}_z = \tilde{e}_z(x)\exp(iky\sin\theta)$ (where $k = \frac{2\pi}{\omega}$) while in P polarization, one follows components $\tilde{E}_y$ and $\tilde{E}_x$ written as $\tilde{E}_y = \tilde{e}_y(x)\exp(iky\sin\theta)$ and $\tilde{E}_x = \tilde{e}_x(x)\exp(iky\sin\theta)$, respectively. Methods for numerically calculating the electric field in such stratified media exist (see [19,20]). Thanks to the *optical reciprocity theorem*, the methodology used to calculate the pump field and the fluorescence field is the same. Indeed, this theorem stipulates that when a monochromatic plane wave from a point source at position B far away from the sample generates an electric field intensity I at a point A inside the sample, the same intensity will be encountered at B when the source is moved to A [21,22]. In our context, atoms that fluoresce inside the sample now become the points source of radiation, excited by the XFEL which plays no role in further processes since it differs in energy from the fluorescence energy. The electric field intensity produced in all of space by the internal source

is supposed to be measured at infinity. Finally, calculating an electric field of fluorescence E at depth x in the layered structure for a glancing angle θ_{out}, in the same way as that for the pump field, but at ω_f, one obtains the fluorescence intensity at infinity away from the sample I_f as

$$I_f = \int j(x)|E(x,\theta_{\text{out}})|^2 dx, \tag{2}$$

where $j(x)$ is the fluorescence emissivity at x (induced by the pump). $j(x)$ is proportional to the population of the upper level of the fluorescent transition and to the corresponding Einstein coefficient. One sees here that, equivalently to the Purcell effect [23] which describes the modification of the spontaneous decay rate in a cavity (an effect evidenced for single atoms [24]), the *effective* local emissivity $j(x)|E(x,\theta_{\text{out}})|^2$ incorporates this effect. Indeed, a classical treatment of this effect consists in multiplying the transition rate (as obtained in vacuum by the Fermi's golden rule) by the density of mode (DOM) in the cavity. Moreover, it has been shown that the computation of a cavity-induced emission rate can be carried out as well classically and quantum electrodynamically [25–27]. Hence, since instead of the DOM one uses equivalently the local intensity in the multilayered structure, our definition of the *effective* local emissivity incorporates the Purcell effect.

One considers now the basic ingredient of Eq. (1), namely, the complex refractive index at wavelengths λ_p or λ_f. $\tilde{n}$ is written as $\tilde{n} = 1 - \delta - i\beta$ and its parts read [28] $\delta = \frac{r_o \lambda_{p,f}^2}{2\pi} N f_1$ and $\beta = \frac{r_o \lambda_{p,f}^2}{2\pi} N f_2$. N is the density of atoms, and r_o is the classical electron radius. f_1 and f_2 are the real and the imaginary parts of the atomic scattering factor. They are linked to the local opacity per atom $\kappa(\omega)$ through the relations

$$f_1(\omega_{p,f}) = Z^* + \hbar b \int \frac{\omega^2 \kappa(\omega)}{\omega_{p,f}^2 - \omega^2} d\omega \tag{3}$$

and

$$f_2(\omega_{p,f}) = \frac{\pi}{2} \omega_{p,f} \hbar b \kappa(\omega_{p,f}), \tag{4}$$

where $b^{-1} = \pi h c r_o$, and Z^* is the atomic number Z corrected for relativistic effects. More precisely, $Z^* = Z - E_{\text{tot}}/mc^2$, where E_{tot} is the total binding energy of the atomic electrons while mc^2 is the electron rest mass. Different fits of E_{tot} may be used [28,29]. In Eq. (3), the integral is defined in the "principal value" sense and special care is required when performing numerical evaluations [30]. There exists the possibility for part β to be negative. From Eq. (4), this corresponds to the case where the opacity is negative. In other words, the opacity becomes a *gain* at some frequencies. This may be the case if the external pump (at ω_p) induces a strong population inversion between two specific levels corresponding to the fluorescence transition under study and whose energy difference is denoted $\hbar\omega_f$. Determination of this opacity relies on a preliminary calculation of the local population kinetics resulting from the XFEL photon absorption. During a single pulse, various microscopic processes occur in addition to photoionization. Fluorescence (and more generally, radiative relaxation) is one of the processes. Autoionization (which strongly competes with fluorescence) is another process. Both photoionization and autoioinization are responsible of the production of free electrons called photoelectrons and Auger electrons, respectively. These electrons may induce subsequent collisional processes such as collisional ionization and excitation. A consistent treatment of all of these processes requires a proper collisional-radiative modeling to be performed inside each cell of the material, at each time step during the interaction and the process of emission. This particular aspect of the modeling is described in detail elsewhere [31–33]. More precisely, we work here in the configuration average (CA) approximation for the description of atomic structure. All the rates for the collisional and radiative processes are calculated within this CA framework [34]. The choice of relevant (active) configurations depends on the XFEL photon energy [33].

At each instant, the incident XFEL electric field map in the material (as obtained by solving the Helmholtz wave equation in the material) allows one to obtain the energy deposition on the free electrons (Joule-Lenz law). Assuming a quasi-instantaneous thermalization of these free electrons (which is true in solids at least for low-energy photoelectrons and Auger electrons), one may define by means of a convenient equation of state, a local electron temperature. Subsequently, this temperature map is used to build and solve a new rate-equation system in each cell. In this way, a consistent treatment of the population kinetics and of the XFEL energy deposition and pumping, is performed. It is possible to evaluate an energy transfer between the electron and the ion subsystems, and ultimately, a hydrodynamics motion. But this occurs on a timescale (∼1 ps) greater than the XFEL pulse, i.e., well after the effects studied in the present article.

We complete this section by discussing the relevance of this theoretical approach in the context of a strong enhancement of a fluorescence emission, which is the subject of this article. It is important to note that, even though the propagation effects are neglected in our very thin samples, a time dependence is introduced in the refractive indices through the opacity [see Eqs. (3) and (4)]. This opacity is built from the atomic populations and especially those involved in the population inversion induced by the XFEL. Therefore, our approach is basically a *rate equation approach*. Also, emitted radiation is treated as a time-dependent intensity through the square of the electric field. Besides the "cavity effect" of a multilayer (as we will discuss below) and when amplification occurs, the time-dependent intensity is directly determined by the population inversion and not by a macroscopic polarization buildup related to this population inversion and to the coherences. Treating in these conditions, the emitted radiation as an intensity, compared with a treatment of the complex electric polarization buildup on the amplified transition, as in the Bloch-Maxwell (BM) approach, leads to a loss of information. Consequently, when amplification occurs, our *rate-equation approach* gives only an estimate of the total output intensity. It is clear that a more correct modeling would require a solution of the Bloch-Maxwell equations (see, for instance, [35]), although, in our conditions (dense and more or less heated media), coherences are probably destroyed by dephasing effects. Nevertheless, a BM treatment would incorporate propagation effects, necessary in an extended medium [35].

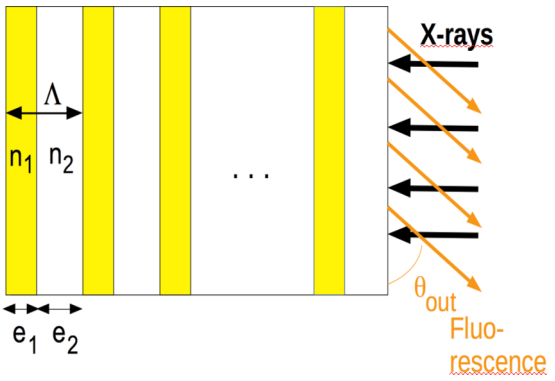

FIG. 2. Sketch of a stack of bilayers (of two different elements) excited by x rays above an absorption edge (K, L, or M) in one of the two elements. This results in a $K\alpha, \beta$, $L\alpha, \beta, \gamma, \ldots$, or $M\alpha$ fluorescence emission which can be observed as a function of a glancing angle θ_{out}. Thicknesses of a bilayer are e_1 and e_2, respectively, while refractive indices are n_1 and n_2, respectively. The period is $\Lambda = e_1 + e_2$.

III. GRAZING EXIT X-RAY FLUORESCENCE AND KOSSEL DIFFRACTION

A. Low fluence excitation

We discuss a few phenomena concerning the x-ray fluorescence of an externally excited layered material. We restrict ourselves here to x-ray fluorescence from monolayer or periodic multilayer materials as depicted in Fig. 2 for the case of a stack of bilayers. We first consider a sample consisting in a stack of 30 bilayers (Mg/Co) of thicknesses $e_1 = 5.45$ nm and $e_2 = 2.55$ nm, respectively. This sample has already been considered in the context of excitation by synchrotron radiation [36]. It will be considered below in the context of intense irradiation. If Mg layers are considered as *active*, i.e., *K-shell photoionized* by some external source (e.g., an XFEL), the level scheme is depicted in Fig. 3. What is discussed in this paragraph, is the case of *low fluence excitation*. What we mean here is an external excitation high enough to induce a noticeable fluorescence while the refractive indices of the material remain unaffected by the excitation field (no significant heating and modification of the cold atomic populations).

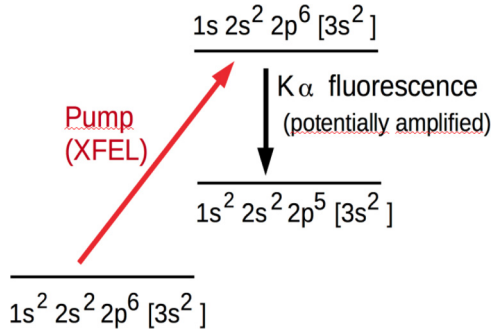

FIG. 3. Main levels (of solid Mg) involved in a pumping-fluorescence scheme. Other collisional-radiative couplings (not shown) are taken into account in the modeling. In solid density Mg (cold or hot), $[3s^2]$ electrons are delocalized free electrons.

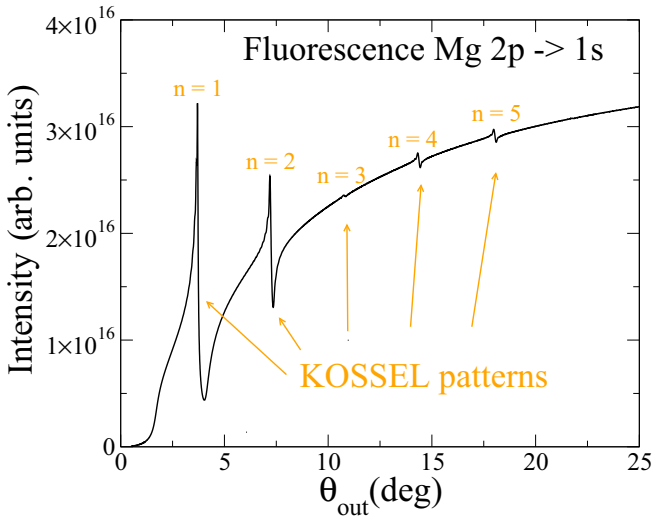

FIG. 4. Calculated angular scan for the Mg $K\alpha$ line emitted by a stack $(\text{Mg/Co})_{30}$ ($e_1 = 5.45$ nm and $e_2 = 2.55$ nm) irradiated by x rays above the Mg K edge. Kossel patterns are labeled by their Bragg order n.

At low excitation fluence above the Mg K edge (1303 eV), an angular scan of the fluorescence intensity at the Mg $K\alpha$ energy (1253.6 eV) is displayed in Fig. 4. This fluorescence intensity is calculated from Eq. (2) in which the map $E(x, \theta_{\text{out}})$ of the fluorescent electric field is obtained by solving the wave equation (1) with a fixed set of complex refractive indices for the two elements of the multilayer. Here, these fixed refractive indices are deduced from a *cold* opacity [see Eqs. (3) and (4)]. In these conditions, we checked that these indices were very close to the values given on the Center for X-ray Optics (CXRO) website [37]. Last, the $K\alpha$ emissivity is supposed to be the same over the whole sample which supposes a uniform excitation. One observes specific structures at the Bragg angles of the multilayer. These modulations of the outgoing emission come from interferences due to the diffraction processes inside the periodic material. They correspond here to the so-called Kossel patterns [9,38–40] as mentioned in the Introduction. One can observe the same structures for the same kind of multilayer sample but assuming now an excitation above the K edge of cobalt (7709 eV). Using the same calculation procedure as for Fig. 4, one can see in Fig. 5, that the angular scan of the Co $K\alpha_1$ fluorescence (6930.3 eV) shows Kossel patterns depending on the considered stack $(\text{Mg/Co})_N$ (here, $e_1 = e_2 = 2.5$ nm, and $N = 50$ and 100). Even in this context of low fluence excitation, one sees that the difference in intensity does not depend linearly on the number of emitting atoms. Other effects such as reabsorption play a role.

While previous patterns are the consequence of the juxtaposition of layers having different refractive indices, it is interesting to discuss a simple finite thickness effect which can be observed at angles around the critical angle. Figure 6 displays an angular scan of the Co $K\alpha$ fluorescence for three monolayer Co samples of three different thicknesses. Again, the calculation procedure is the same as for Fig. 4. Like x-ray fluorescence from bulk materials, emission from the thicker

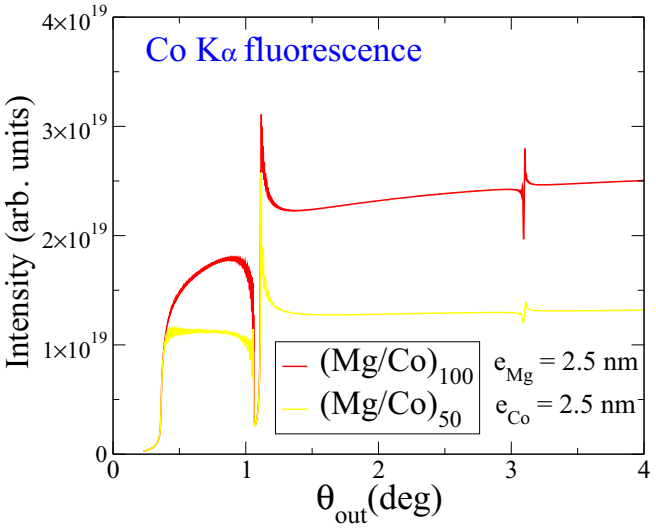

FIG. 5. Calculated angular scan for the Co $K\alpha$ line emitted by two stacks $(Mg/Co)_{50}$ and $(Mg/Co)_{100}$ irradiated by x rays above the Co K edge.

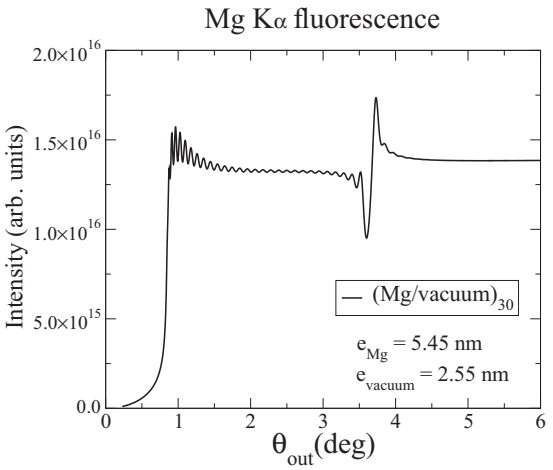

FIG. 7. Calculated angular scan for the Mg $K\alpha$ line emitted by a stack $(Mg/vacuum)_{30}$. A uniform excitation (K-shell hole production) has been supposed through the whole sample.

sample (500 nm) does not display any modulations. On the contrary, angular dependence of the intensity for thinner samples shows characteristic oscillations due to interferences. This effect is a characteristic aspect of the GEXRF. As a final comment, Fig. 7 shows a clear occurrence of both GEXRF effects (for θ_{out} around 1°) and Kossel diffraction (around 3.5°) for a juxtaposition of magnesium layers separated by vacuum layers ($\tilde{n} = 1$). In principle, the two effects should mix if the period Λ of the material is increased so that the Bragg angle is comparable to the critical angle.

B. Strong x-ray pumping

Up to now, we discussed cases where refractive indices in the material (whether it is a multilayer or not) are not affected by the excitation device. Here we discuss the case of an *active* medium where in particular, the imaginary part β is made negative (at some frequencies) by some means. As seen in Sec. II, this means that the absorption coefficient becomes negative. In the case of multilayer materials, this situation has already been considered in the past and the possibility of x-ray laser oscillations has been examined [41,42]. In particular, it is shown that the reflectivity of an N-period stack presents some poles for some values of the gain (negative absorption) in one material of the stack. We just illustrates this possibility numerically for the case of a multilayer material previously considered, namely, the stack $(Mg/Co)_{30}$, but where we artificially modified the β part of the refractive index of Mg. Such numerical solutions of the wave equation (1) with an artificially modified complex refractive index are displayed in Fig. 8. What is shown is the square of the electric field at the Mg $K\alpha$ wavelength and the first Bragg angle (see Fig. 4), inside a $(Mg/Co)_{30}$ stack (i.e., as a function of x) and for different values of the imaginary part of the refractive index of magnesium. What is remarkable is the typical resonatorlike

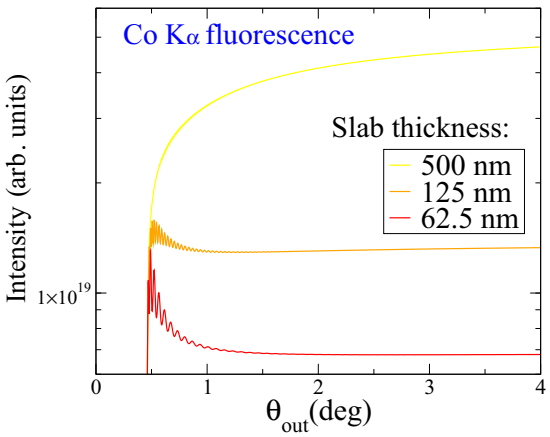

FIG. 6. Calculated angular scan around the critical angle for the Co $K\alpha$ line emitted by slabs of different thicknesses. A preliminary uniform excitation (K-shell hole production) has been supposed over the whole slabs.

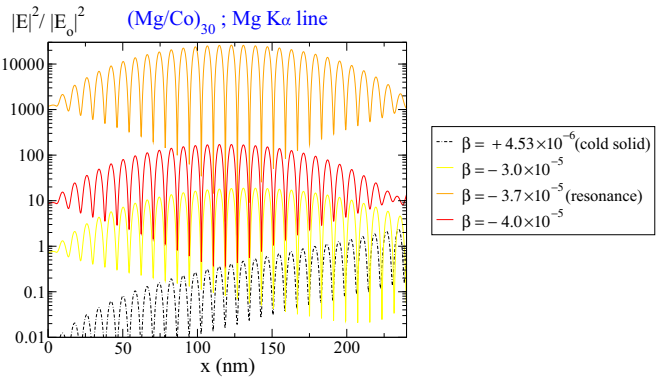

FIG. 8. Square of the electric field at the Mg $K\alpha$ energy (1253.6 eV) inside the $(Mg/Co)_{30}$ stack ($e_1 = 5.45$ nm, $e_2 = 2.55$ nm), for different imposed values of the imaginary part of the refractive index in the Mg layers. Here, $\tilde{n}_{Mg} = 1–1.521\,49 \times 10^{-4} - i\beta$ while $\tilde{n}_{Co} = 1–9.991\,87 \times 10^{-4} - i3.970\,76 \times 10^{-4}$. Results are normalized to an incident intensity $|E_o|^2$.

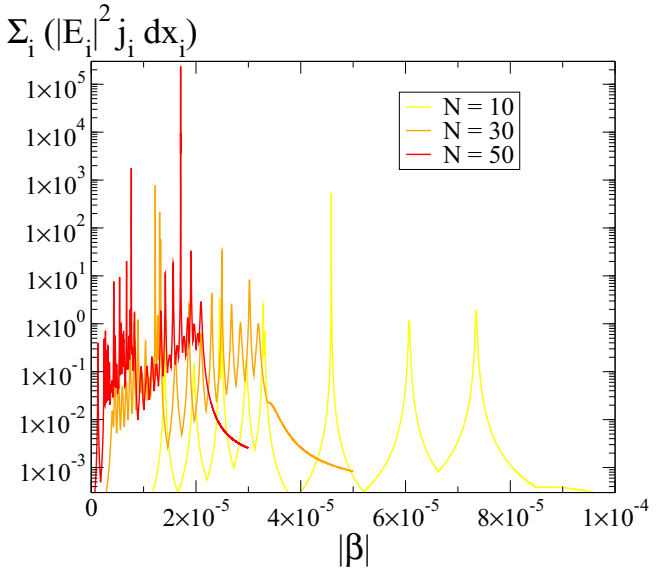

FIG. 9. Maximum of the emerging intensity on the Co $K\alpha_1$ found in a glancing angular interval around the first Bragg angle ($\theta_B = 1.025^\circ$) as a function of the imaginary part of the refractive index of Co. Three stacks $(Mg/Co)_N$ with $e_1 = 2.5$ nm, $e_2 = 2.5$ nm, and $N = 10, 30, 50$ are considered. Here the pumping is uniform, i.e., arbitrarily $j_i = 1$ for all cells i.

aspect of the electric field which is observed for some values of β, e.g., for $\beta = -3.7 \times 10^{-5}$ and $\beta = -4 \times 10^{-5}$. One sees here how the periodic structure of the multilayer provides feedback by Bragg coupling between the forward and backward traveling waves, so that the multilayer behaves as a spatially distributed resonator in this x-ray range. Thus, strong values of the calculated field suggests the possibility of a strong amplification of the Mg $K\alpha$ fluorescence if a strong population inversion is realized on this transition despite the absorption in the other intervening layers of cobalt. Of course, the pumping intensity must be considerable and supplied by x-ray bursts of short duration.

To pursue our numerical study and for the subsequent discussions, it is instructive to select a small angular interval around the first Bragg angle (where the resonance takes place) and to track the maximum of intensity emerging from the multilayer as a function of the imaginary part of the refractive index. This is done in Fig. 9, which displays the maximum of intensity of the Co $K\alpha_1$ line emerging from the multilayers $(Mg/Co)_N$ ($N = 10, 30, 50$), as a function of β. Here $e_1 = 2.5$ nm, $e_2 = 2.5$ nm, the glancing angular interval is centered around the first Bragg angle, and the emissivity of each cell is arbitrarily set to 1. What we note is a nonmonotonic behavior of the emerging intensity which, in this particular case, reflects the existence of poles in the reflectivity as mentioned above. While the number of poles is equal to N [41], intensities strongly vary with N. If one uses an x-ray pump of sufficient intensity but varying in time (e.g., a Gaussian pulse), one necessarily makes a scan in β which crosses resonance regions as indicated in this figure. Of course, a spatial inhomogeneity of the pumping is likely to make this behavior even more complex.

IV. AMPLIFIED FLUORESCENCE IN REAL CONDITIONS OF XFEL PUMPING

In this section, we place ourselves in more realistic conditions of pumping by an XFEL since these sources provide short bursts of intense radiation. In the presented simulations, the XFEL pulse is supposed Gaussian and of 10 fs duration (FWHM). By choosing the pump photon energy just above a K edge, for example, one can expect a large removal of $1s$ electrons so as to create a large population inversion between the atomic core and the filled higher shells. Especially in low-Z elements, it is well known that such core holes relax mainly by autoionization (Auger electron production) rather than radiative deexcitation. However, with a proper collisional-radiative modeling (that includes all possible microscopic effects) which gives the absorption (or gain) coefficient at each instant, one can predict a realistic fluorescence signal more or less amplified by the field effects discussed above. Also, compared with the ideal situation of homogeneous pumping described in the previous section, one has to deal with undesirable but unavoidable effects such as pump attenuation, material heating by photoelectrons and by Auger electrons. These effects contribute to reducing or to destroying the population inversion and the simulations must take into account all of these effects consistently through a computation of the two parts (α, β) of the complex refractive index. So, unlike the calculations of Sec. III where the refractive indices were fixed at their *cold* values, here we follow in time their modifications with the pumping and the heating of the material. This is done both at the XFEL frequency and at the fluorescence frequency according to Eqs. (3) and (4) where the opacity is calculated at each time step. In each cell, this opacity is calculated from the set of populations obtained from a time-dependent collisional-radiative model. Besides the opacity (giving the refractive indices), one also gets the emissivity so that, after a solution of the wave equation (1), the outgoing intensity is computed with Eq. (2). It is clear that, with regard to the geometry depicted in Fig. 2, one expects a larger emission in the backward direction since the XFEL pumping is more efficient in the front layers.

In Fig. 10, we plot a few snapshots of a partial angular scan (around the first Bragg angle) of the Mg $K\alpha$ emission (integrated over the line profile) from a $(Mg/Co)_{30}$ stack when irradiated at normal incidence by a Gaussian pulse of 1332 eV photons, 10 fs duration (FWHM), and having an intensity of 10^{16} W/cm^2. Properties of the multilayer correspond to Fig. 4. Here the intensity is integrated over the whole profile of the Mg $K\alpha$ at 1253.6 eV while the pumping occurs above the K edge (1303 eV) in order to create a large number of $1s$ core holes and to produce a population inversion between $1s$ and the $2p$ shells. It must be noted that in these calculations, we need to solve the Helmholtz wave equation both for the pump and around the Mg $K\alpha$ line which means that at each instant, a preliminary calculation of the refractive indices at the corresponding frequencies has been done in each cell. Of course, these quantities share the same frequency-dependent opacity. In other words, the same atomic physics. What is striking in Fig. 10 is the strong intensity occurring on this first Kossel pattern at one particular instant (here $t = 12.2$ fs). This clearly illustrates the resonator effect provided by the

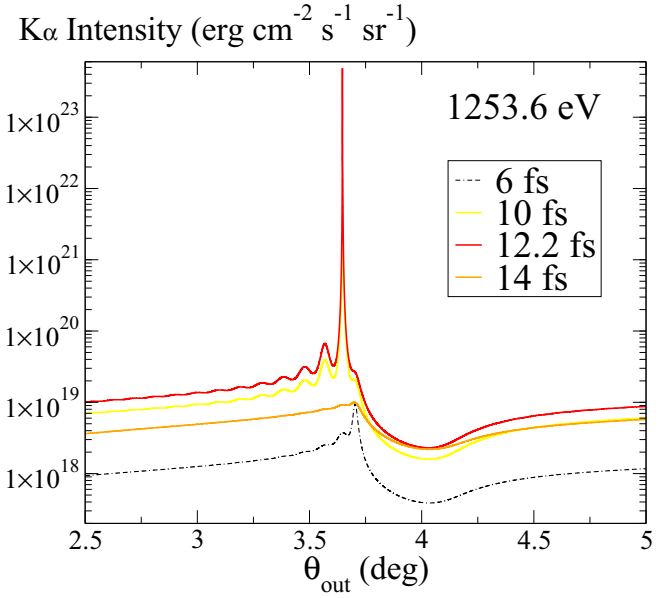

FIG. 10. Snapshots of the outgoing Mg $K\alpha$ emission from a $(Mg/Co)_{30}$ stack in real pumping conditions (1332 eV photons, 10^{16} W/cm^2, FWHM 10 fs, normal incidence). Indicated instants correspond to the time elapsed from the moment the pulse enters the multilayer structure (the peak of the pulse being at 12.8 fs).

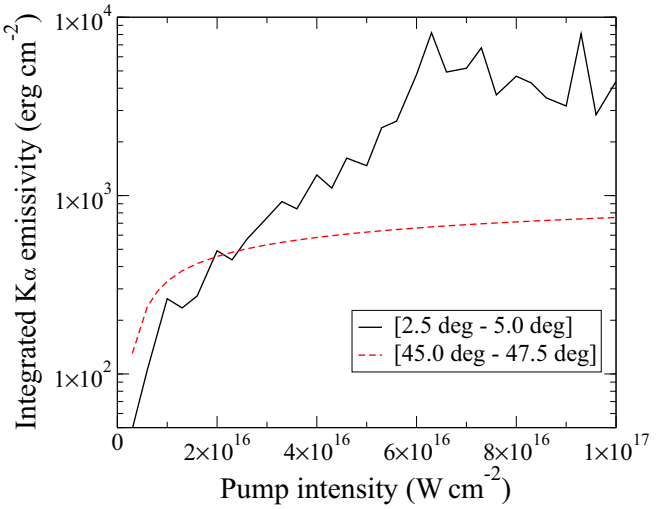

FIG. 12. Time integration (over the pulse) and angular integration of the outgoing Mg $K\alpha$ emissivity as a function the (XFEL) pump intensity for a 10 fs duration Gaussian pulse of 1332 eV photons. The sample is a $(Mg/Co)_{30}$ stack with $e_1 = 5.45$ nm and $e_2 = 2.55$ nm. Solid line: integration on the interval [2.5°–5°] (around the first Kossel pattern). Dashed line: integration on the interval [45°–47.5°] (out of the Kossel directions).

multilayer (see Fig. 7 and its discussion). The fact that this overintensity lasts a very transient time stems from the fact that a condition of resonance for the population inversion (i.e., for β; see for instance, Fig. 9) is reached at some particular instant in the pulse. Another undesirable effect is the heating accompanying the pumping. As explained in the second to last paragraph of Sec. II, our modeling allows an estimation of this heating. Figure 11 displays a profile of the electronic

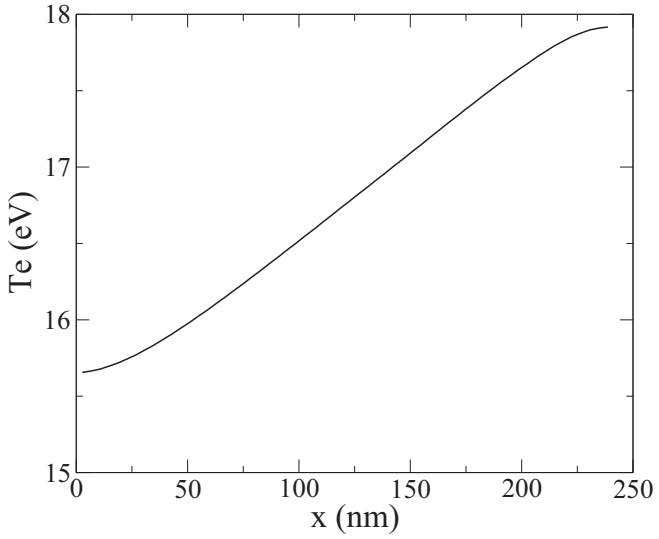

FIG. 11. Spatial profile of electronic temperature at the end of the x-ray pulse, in a $(Mg/Co)_{30}$ stack of period $\Lambda = 8$ nm, irradiated at normal incidence by a Gaussian XFEL pulse at 10^{16} W/cm^2, of 1332 eV photons, and of 10 fs duration (FWHM). The x-ray pulse comes from the right.

temperature in the multilayer, just after the end of the x-ray pulse. One notes a significant heating of the sample (up to 18 eV) in these conditions of irradiation. Also, the heating is not uniform since the sample is irradiated on the right side. This heating modifies the population inversion, i.e., the gain and thus the conditions of resonance in the multilayer. This is why in Fig. 10 a maximum of intensity is observed at about $t = 12$ fs and then a decrease.

A specific amplification feature such as displayed in Fig. 10 occurs in timescales which are too short to be observable. This is why it is interesting to consider the time integration of the fluorescent emission as a function of the pump intensity. Considering the previous multilayer, Fig. 12 displays the results of simulations performed for different pump (XFEL) intensities. Both curves (solid line and dashes) correspond to a time integration of the Mg $K\alpha$ outgoing emissivity but integrated over two different angular intervals. The solid line corresponds to the interval [2.5°–5°], i.e., centered around the first Bragg angle of the multilayer (first Kossel pattern) while the dashed line corresponds to an angular interval [45°–47.5°], completely off the Bragg angles. The overall nonlinear behavior shown by the solid line curve (with respect to the dashed curve) illustrates well the amplification which is a consequence of the resonator effect discussed previously. For the higher pump intensities, one observes a somewhat erratic behavior of the emission. This complex behavior is a combination of different effects. First, the photoionization pumping is not homogeneous since it is realized from one side. As a consequence, the resonance regions (see Fig. 9, for instance) are reached at different times and at different places in the sample. Also, there is an overheating of the sample (destroying the population inversion) occurring also at different times and different places.

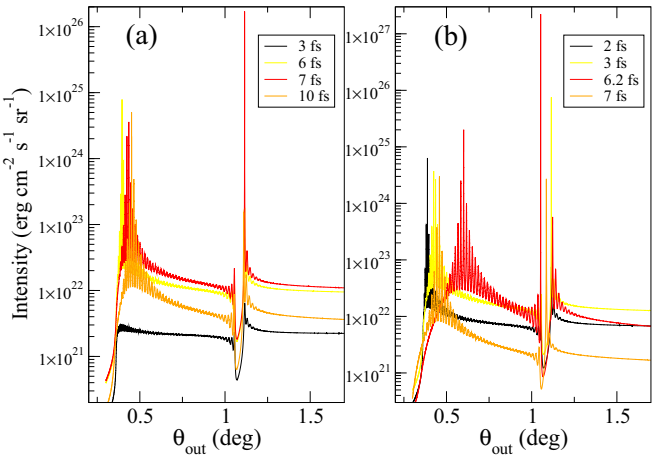

FIG. 13. Snapshots of the grazing outgoing Co $K\alpha_1$ emission from a $(Mg/Co)_{50}$ stack ($e_1 = e_2 = 2.5$ nm) in real pumping conditions (7720 eV photons, FWHM 10 fs, normal incidence). (a) 6×10^{18} W/cm^2. (b) 3×10^{19} W/cm^2.

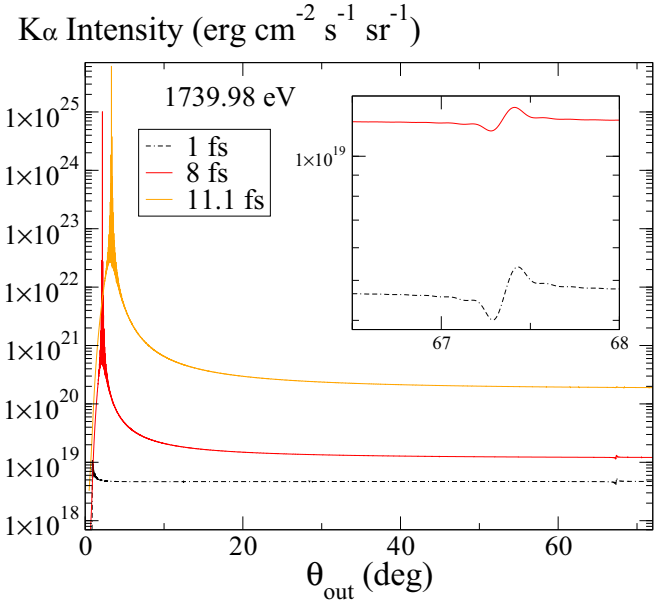

FIG. 14. Angular scan of the Si $K\alpha$ emission, at different times during the irradiation of the stack $(Si/vacuum)_{1000}$ ($e_1 = 0.1309$ nm, $e_2 = 0.2541$ nm) by a 10^{17} W/cm^2 pulse, 10 fs long, of 1900 eV photons. The inset is a zoom on the Kossel diffraction region around 67°.

Still on the same kind of multilayer, we examined the possibility of an amplification of the Co $K\alpha$ emission, i.e., in a harder x-ray range since the Co $K\alpha_{1,2}$ are at 6930.3 and 6915.3 eV, respectively (the K edge being at 7709 eV). The pump considered here is a Gaussian pulse of 7720 eV photons, 10 fs duration (FWHM), and having an intensity of 6×10^{18} W/cm^2 and 3×10^{19} W/cm^2, respectively. It arrives at normal incidence on the stack $(Mg/Co)_{50}$, with $e_1 = e_2 = 2.5$ nm (so that the period $\Lambda = 5$ nm). Figure 13 displays a few snapshots of an angular scan of the Co $K\alpha_1$ line emission during the pulse, for these two XFEL intensities. For this $K\alpha_1$ energy, the first Bragg angle is 1.03°. What is observed here is a competition between the Kossel diffraction and the GEXRF effects, the critical angle θ_c being at about 0.4°. About the latter, one observes an angular shift in the maximum of emission. This shift is due to the strong modification of refractive index due to the heating in the material. About the Kossel patterns, one notes an increase by a factor 10 on the intensity while the pump intensity has increased by a factor 5.

Previous calculations were based on the use of artificial layered media. It turns out that the same considerations about Kossel diffraction can be applied to natural crystals if one uses the accidental periodicities (between atomic layers) which fufill the Bragg conditions. Crystal periodicities are usually in the range of a few tenths of nanometers. Then, one can expect normal or not so grazing directions of oscillation feedback for wavelengths in this typical range. For instance, if one considers a Si crystal whose planes parallel to the surface are (110), atomic layer spacing $d = 0.385$ nm gives a Bragg angle of 67.73° for the Si $K\alpha$ line at 1740 eV. The problem here is that the thickness for an efficient pumping may be too small for ensuring a non-negligible reflectivity at the Bragg angle in the keV range. In order to explore both GEXRF amplification and Kossel amplification effects in a natural crystal, we considered different slabs of (110) Si. To introduce the periodicity in our calculations, we used the model where the crystal (supposedly perfect) is approximated by a stack of bilayers of period d where the first layer is a layer of Si atoms whose thickness corresponds to the size of the Si atoms while the second layer is an empty layer of index 1. This vacuum layer acts as an ideal nonabsorber. In our calculations, we choose the thickness of the Si atom layer to be $0.34d$. Figure 14 displays an angular scan at different times of the Si $K\alpha$ line emitted by a 0.385-μm-thick layer of Si irradiated by a pulse of 10^{17} W/cm^2, 10 fs duration, and 1900 eV of photon energy (i.e., above the Si K edge). More precisely, the multilayer considered here consists in the stack $(Si/vacuum)_{1000}$ with $e_1 = 0.1309$ nm and $e_2 = 0.2541$ nm.

What is noticeable in this case is mainly the presence of amplified GEXRF structures as the emission in the Bragg diffraction region (Kossel region) around 67° remains very weak. This is due to a reflectivity at the Bragg angle which remains very low for this sample thickness. To see an enhancement of this emission and possibly a feedback effect, we performed another calculation in the same conditions but for the stack $(Si/vacuum)_{10\,000}$. Now, the total thickness is of 3.85 μm, i.e., at the limit of validity of our treatment where we do not take into account propagation effect. Results are shown in Fig. 15. While Kossel emission remains low compared with the grazing emission, it is clearly noticeable and indicates a resonator or feedback effect. Here, a further comment concerns the transmission of the pump (at 1900 eV) of the Si sample. For a thickness of 3.85 μm, the transmission is less than 10%, which suggests a very nonuniform profile of absorption.

Always with the aim of increasing the $K\alpha$ emission, and as suggested elsewhere [43], it is interesting to change the geometry of the problem, i.e., by referring to Fig. 1, pump along the y axis a thin quantity of matter (∼0.1 μm), but still keeping the direction of stratification along the x axis. The results of such simulations are displayed in Fig. 16 for the stack $(Si/vacuum)_{5000}$ (1.92 μm) and 2 XFEL pulse intensities. In

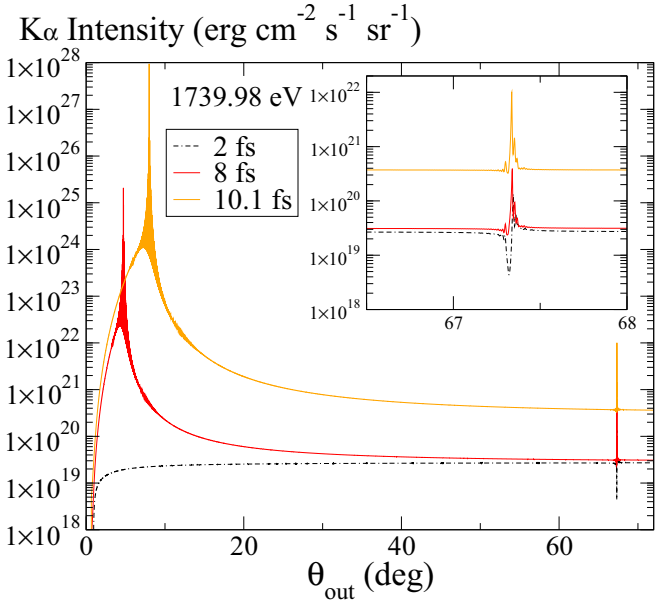

FIG. 15. Angular scan of the Si $K\alpha$ emission, at different times during the irradiation of the stack $(\mathrm{Si/vacuum})_{10\,000}$ ($e_1 = 0.1309$ nm, $e_2 = 0.2541$ nm) by a 10^{17} W/cm^2 Gaussian pulse, 10 fs duration (FWHM), of 1900 eV photons. The inset is a zoom on the Kossel diffraction region around 67°.

these conditions of homogeneous pumping along the x axis, one sees an increase of the Kossel pattern intensity by a factor 10 000 while the pump intensity has increased by a factor 10, which means that a strong feedback effect takes place around the Bragg angle. In order to evaluate possible saturation effects in these conditions, a calculation of the (local) forward $K\alpha$ intensity (in addition to the backward intensity) has been implemented. This allowed one to build the mean integrated intensity which is involved in the rate-equation system for estimating both absorption and stimulated emission rates. We did not see any effect of these terms, which indicates that saturation is not yet effective in these conditions. Then, results are likely to be more spectacular for thicker samples (along x), The problem now is that one cannot ignore propagation effects. We leave this problem for future studies.

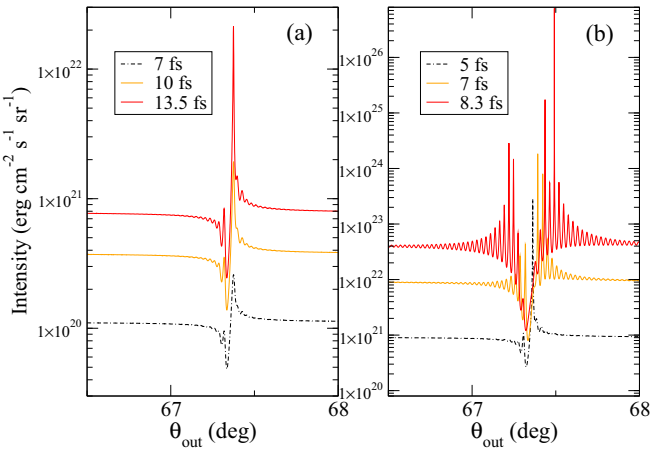

FIG. 16. Angular scan of the Si $K\alpha$ emission, at different times during the transverse irradiation (along the y axis; cf. Fig. 1) of the stack $(\mathrm{Si/vacuum})_{5000}$ ($e_1 = 0.1309$ nm, $e_2 = 0.2541$ nm) by Gaussian pulses, 10 fs duration (FWHM), of 1900 eV photons. (a) 10^{16} W/cm^2. (b) 10^{17} W/cm^2. Thickness (along the y axis) is less than 1 μm.

V. CONCLUSIONS

We performed a computational study of the x-ray fluorescence induced by the irradiation (pumping) of thin layered media by intense, short x-ray pulses. Indeed, it turns out that the power density deliverable by XFELs is sufficient to create strong population inversions in the x-ray range and also that important field enhancements due to interferences can be expected at grazing angles of observation. Furthermore, using a multilayer material (or a periodic system) both as an emitter and a resonator, may also strongly enhance the emission at the Bragg angles of the multilayer. For simulations, we solved the Helmholtz wave equation both for the x-ray pump and for the fluorescence signal. At each time step during the pump pulse, complex refractive indices are calculated from a consistent treatment of x-ray absorption and of atomic physics. Taking periodic multilayers made of a stack of Mg/Co bilayers as a typical sample, we evidenced strong amplifications of either the $K\alpha$ line of Mg or the $K\alpha$ line of Co, depending on irradiation conditions. In this x-ray region where the first Bragg angle is not so far from the total reflection region, we observed a competition between the so-called GEXRF and the Kossel emission which can be subjected to feedback. Independently, we considered the problem of single crystals (here Si) which offer a natural periodicity. Because of the difficulty of realizing a uniform and constant pumping, fluorescence emission encompasses different complex phenomena. This results in an outgoing emission which is strongly time dependent (over the XFEL pulse duration). Furthermore, it seems that a compromise between a large intensity (needed for an efficient pumping) and the subsequent undesirable heating of the material has to be found. Dealing with high-energy photoelectrons, i.e., choosing a pump photon energy well above the edge of interest could be a solution because these electrons (which, along with Auger electrons, are responsible for the heating) are transported in regions far away from the deposition of the x rays. Also a pulse shaping of the XFEL could help in realizing an optimal pumping.

We point out that a better control of feedback effects in the x-ray range would help in the context of valence-to-core spectroscopy (for structural studies). Indeed, an optimization of these effects offers the opportunity to observe these usually very weak transitions.

Finally, while these conditions are probably difficult to find, one can imagine a configuration where the buildup of the stimulated fluorescence is able to beat the Auger relaxation and where most of the emission occurs in a prevailing direction such as a Bragg direction.

ACKNOWLEDGMENTS

At numerous times during the course of this work, O.P. has benefited from discussions and helpful advice concerning the use of computational resources from Paul Genesio at PIIM laboratory.

[1] B. W. Adams *et al.*, J. Mod. Opt. **60**, 2 (2013).

[2] B. W. Adams, *Nonlinear Optics, Quantum Optics and Ultrafast Phenomena with X-Rays* (Kluwer Academic, Norwell, MA, 2008).

[3] F. Vagizov, V. Antonov, Y. V. Radeonychev, R. N. Shakhmuratov, and O. Kocharovskaya, Nature (London) **508**, 80 (2014).

[4] R. Röhlsberger, H.-C. Wille, K. Schlage, and B. Sahoo, Nature (London) **482**, 199 (2012).

[5] J. Wang, M. J. Bedzyk, and M. Caffrey, Science **258**, 775 (1992).

[6] J. Haber, J. Gollwitzer, S. Francoual, M. Tolkiehn, J. Strempfer, and R. Röhlsberger, Phys. Rev. Lett. **122**, 123608 (2019).

[7] T. Noma, A. Iida, and K. Sakurai, Phys. Rev. B **48**, 17524 (1993).

[8] Y.-C. Tu, Y.-Y. Yuan, K. Le Guen, J.-M. André, J.-T. Zhu, Z.-S. Wang, F. Bridou, A. Giglia, and P. Jonnard, J. Synchrotron. Radiat. **22**, 1419 (2015).

[9] E. Langer and S. Däbritz, IOP Conf. Proc. No. **7**, 012015 (2010).

[10] K. Le Guen *et al.*, J. Nanosci. Nanotechnol. **19**, 593 (2019).

[11] J. Zegenhagen and A. Kazimirov, editors, *The X-Ray Standing-Wave Technique. Principles and Applications* (World Scientific, Singapore, 2013).

[12] A. X. Gray *et al.*, Phys. Rev. B **82**, 205116 (2010).

[13] M. J. Bedzik, *X-Ray Standing-Wave Studies of the Liquid/Solid Interface and Ultrathin Organic Films*, in Surface X-Ray and Neutron Scattering Vol. 51, edited by H. Zabel and I. K. Robinson (Springer-Verlag, Berlin, 1992).

[14] N. Rohringer *et al.*, Nature (London) **481**, 488 (2012).

[15] M. Beye, S. Schreck, F. Sorgenfrei, C. Trabant, N. Pontius, C. Schüßler-Langeheine, W. Wurth, and A. Föhlisch, Nature (London) **501**, 191 (2013).

[16] H. Yoneda *et al.*, Nature (London) **524**, 446 (2015).

[17] P. Jonnard, J.-M. André, K. Le Guen, M. Wu, E. Principi, A. Simoncig, A. Gessini, R. Mincigrucci, C. Masciovecchio, and O. Peyrusse, Struct. Dyn. **4**, 054306 (2017).

[18] T. Kroll, C. Weninger, R. Alonso-Mori, D. Sokaras, D. Zhu, L. Mercadier, V. P. Majety, A. Marinelli, A. Lutman, M. W. Guetg *et al.*, Phys. Rev. Lett. **120**, 133203 (2018).

[19] Z. Knittl, *Optics of Thin Films* (Wiley, London, 1976).

[20] L. A. A. Pettersson, L. S. Roman, and O. Inganäs, J. Appl. Phys. **86**, 487 (1999).

[21] W. Schülke and O. Brümmer, Z. Naturforsch. A **17**, 208 (1962).

[22] M. Born and E. Wolf, *Principles of Optics* (Pergamon, New York, 1975).

[23] E. M. Purcell, Phys. Rev. **69**, 674 (1946).

[24] P. Goy, J. M. Raimond, M. Gross, and S. Haroche, Phys. Rev. Lett. **50**, 1903 (1983).

[25] H. Morawitz, Phys. Rev. **187**, 1792 (1969).

[26] H. Chew, Phys. Rev. A **38**, 3410 (1988).

[27] J. P. Dowling, M. O. Scully, and F. De Martini, Opt. Commun. **82**, 415 (1991).

[28] B. L. Henke, E. M. Gullikson, and J. C. Davis, At. Data. Nucl. Data Tables **54**, 181 (1993).

[29] M. Kefi, J. M. André, Y. Heno, G. Giorgi, and C. Bonnelle, Phys. Rev. A **45**, 2859 (1992).

[30] K. Ohta and H. Ishida, Appl. Spectrosc. **42**, 952 (1988).

[31] O. Peyrusse, Phys. Rev. E **86**, 036403 (2012).

[32] H.-K. Chung, S. B. Hansen, and H. A. Scott, *Generalized Collisional-Radiative Model Using Screened Hydrogenic Levels*, in Modern Methods in Collisional-Radiative Modeling of Plasmas, edited by Yuri Ralchenko (Springer, New York, 2016), Chap. 3.

[33] O. Peyrusse, in *Collisional-Radiative Modeling and Interaction of Monochromatic X-Rays with Matter*, edited by Yuri Ralchenko, Modern Methods in Collisional-Radiative Modeling of Plasmas (Springer, New York, 2016), Chap. 6.

[34] O. Peyrusse, J. Phys. B: At., Mol. Opt. Phys. **32**, 683 (1999).

[35] C. Weninger and N. Rohringer, Phys. Rev. A **90**, 063828 (2014).

[36] P. Jonnard, Y.-Y. Yuan, K. Le Guen, J.-M. André, J.-T. Zhu, Z.-S. Wang, and F. Bridou, J. Phys. B **47**, 165601 (2014).

[37] CXRO, http://www.cxro.lbl.gov/.

[38] T. Gog, D. Bahr, and G. Materlik, Phys. Rev. B **51**, 6761 (1995).

[39] P. Jonnard, J.-M. André, and C. Bonnelle, Appl. Phys. Lett. **81**, 1524 (2002).

[40] P. Jonnard, J.-M. André, C. Bonnelle, F. Bridou, and B. Pardo, Phys. Rev. A **68**, 032505 (2003).

[41] A. Yariv and P. Yeh, Opt. Commun. **22**, 5 (1977).

[42] J.-M. André, K. Le Guen, and P. Jonnard, Laser Phys. **24**, 085001 (2014).

[43] A. Yariv, Appl. Phys. Lett. **25**, 105 (1974).